American Mineralogist, Volume 82, pages 452–459, 1997

High-pressure behavior of kyanite: Compressibility and structural deformations

PAOLA COMODI,[1] PIER FRANCESCO ZANAZZI,[1] STEFANO POLI,[2] AND MAX W. SCHMIDT[3]

[1]Dipartimento di Scienze della Terra, Università di Perugia, Piazza Università, I-06100 Perugia, Italy
[2]Dipartimento di Scienze della Terra, Università di Milano, Via Botticelli 23, I-20133 Milano, Italy
[3]CNRS-URA 10, Magmas and Volcans, 5 Rue Kessler, 63038 Clermont-Ferrand, France
also at: Bayerisches Geoinstitut, 95440 Bayreuth, Germany

ABSTRACT

The lattice parameters of kyanite were measured at various pressures up to about 60 kbar by single-crystal X-ray diffraction in a diamond anvil cell. Unit-cell dimensions decreased linearly with an almost uniform rate:

$\beta_a = 2.00(8) \times 10^{-4}$, $\beta_b = 1.90(4) \times 10^{-4}$, $\beta_c = 2.00(4) \times 10^{-4}$ kbar^{-1}. The principal compressibility coefficients were $\beta_1 = 2.23 \times 10^{-4}$, $\beta_2 = 2.04 \times 10^{-4}$, $\beta_3 = 1.65 \times 10^{-4}$ kbar^{-1}, with β_1 forming an angle of 35° with the *c* axis. K_0, calculated by fitting pressure-volume data to a third-order Birch-Murnaghan equation of state, was 1560(100) kbar, with K' 5.6(5.5); when K' was set at 4, K_0 became 1600(30) kbar.

Structural refinements were carried out on data collected at 0.001 kbar with the crystal in air and at 0.1, 25.4, 37, and 47 kbar with the crystal in the diamond anvil cell. Whereas the Si tetrahedra and Al4 octahedron were incompressible in this *P* range, the polyhedral bulk modulus for Al1 and Al2 was 1280(150) kbar and 2380(200) kbar for Al3. These octahedra became more regular with increasing pressure.

The almost isotropic compression pattern was due to the many shared edges between the polyhedra, uniformly distributed in the cell. The evolution of Al-Al separation showed that the largest reduction regarded the Al2-Al3 and Al2-Al4 distances, whereas the average Al1-Al2 distance was almost unchanged, resulting from linkage with Si tetrahedra having rigid edges. The result was that the largest reduction did not occur along the *c* axis but along the Al4-Al1–Al2-Al3 directions.

The geometrical structural invariance, expressed by the β_V/α_V ratio and obtained from the average compressibility and average thermal expansion of the cell volume (Winter and Ghose 1979), was 23 °C/kbar. The following equation of state, which applies in crustal *P-T* conditions, may be defined as: $V/V_0 = 1 + 3.00(7) \times 10^{-5}\ T - 5.8(1) \times 10^{-4}\ P$, where *T* is in °C and *P* in kbar.

The present volume-pressure data support multi-anvil experiments by Schmidt et al. (1997) defining the *P-T* conditions necessary for decomposition of kyanite into stishovite + corundum.

INTRODUCTION

Kyanite, andalusite, and sillimanite, the three polymorphs of Al_2SiO_5, are extensively used to characterize metamorphic rocks. Although the petrologic literature contains numerous attempts at localizing the exact position of the triple point in the *T-P* stability diagram of andalusite-sillimanite-kyanite, small changes in thermodynamic properties greatly influence the position of Al_2SiO_5 phase transitions, and the precise stability fields of the three polymorphs are still uncertain.

Kyanite is the high-pressure polymorph of Al_2SiO_5. In nature, kyanite is a common accessory mineral in eclogite-facies rocks in both metabasaltic and metasedimentary bulk compositions. When such crustal rock types are subducted, kyanite is involved in several breakdown reactions that increase its abundance at pressures higher than 20 kbar. These reactions involve paragonite (Chatterjee 1972), zoisite and lawsonite (Poli and Schmidt 1995), pumpellyite (Schreyer 1988) in mafic rocks, and chloritoid and staurolite in metagreywackes or metapelites (Schreyer 1988).

Neither kyanite nor corundum is reported from typical mantle compositions, i.e., lherzolites or harzburgites. As long as its structure remains stable (to ca. 200 kbar), garnet is capable of hosting the alumina present in an average upper mantle. However, when the subducted slab is disrupted at or below the transition zone, accretion of fertilized peridotite is expected (Ringwood 1991), and Al-phases other than garnet probably play a major role in mantle evolution. Furthermore, in experiments in a laser-heated diamond-anvil cell, Ahmed-Zaid and Madon (1991) identified a new high-pressure form of Al_2SiO_5. This phase, with a structure similar to that of V_3O_5, was proposed as

TABLE 1. Refinement details of kyanite

P (kbar)	0.001	0.1	25.4	37	47
No. measured reflections	1940	1114	1118	1113	1106
No. unique ($I > 3\sigma$)	1660	364	373	359	343
No. parameters	146	65	65	65	65
R_{int}	—	7.6	4.9	7.0	4.0
Scan speed (°/s)	0.12–0.04	0.05	0.05	0.05	0.05
Scan width (°)	2.6	2.4	2.4	2.4	2.4
R%	2.8	8.2	5.9	6.8	8.0

Note: θ range was 3–35° and ω scans were adopted for all data collections.

a candidate for hosting aluminum in the lower mantle. Liu (1974) found that kyanite decomposes to its oxide components, corundum and stishovite, at pressures of 160 kbar and temperatures of 1000–1400 °C. Similar behavior was observed in the germanate analogue of kyanite Al_2GeO_5, which disproportionates at pressures of 70 kbar (Ringwood and Reid 1969).

Despite the importance of kyanite both for thermodynamic data retrieval of high-pressure phases and for subducted slab evolution, equations of state for kyanite are still poorly known. For example, with the exception of preliminary compressibilities determined by Brace et al. (1969) on synthetic pressed aggregates and shock wave data of Marsh (1980), X-ray single-crystal compressibility measurements on this phase are not available. An attempt to determine the bulk modulus of kyanite was made by Irifune et al. (1995) from a thermodynamic analysis of phase equilibrium data based on an experimental study of kyanite decomposition at high pressure and temperature. The aims of the present study, together with a companion paper on the experimental reversal of the kyanite = corundum + stishovite reaction (Schmidt et al. 1997), were to determine the high-pressure behavior of kyanite and to evaluate its thermodynamic properties. This first paper deals with crystal structure modifications at high pressures and the determination of compressibilities through single crystal X-ray diffraction in a diamond-anvil cell. Comparisons of high-pressure and high-temperature data (Winter and Ghose 1979) may also clarify structural evolution with *P* and *T* and the geometric stability of the structure of kyanite to define its equation of state.

EXPERIMENTAL PROCEDURE

The kyanite specimen comes from Minas Gerais, Brazil. Its chemical formula, resulting from the average of several points of SEM-EDS microanalysis, is $Al_{1.98}Fe_{0.02}SiO_5$.

A Merrill-Bassett diamond anvil cell (DAC) with ⅛ carat diamonds of 800 μm as culet face diameter was used for the high-pressure study. Steel foil, 250 μm thick and with a hole of 300 μm diameter, was used as gasket material. A Sm^{2+}-BaFCl powder for pressure calibration (Comodi and Zanazzi 1993) and a 16:3:1 methanol:ethanol:water mixture as pressure-transmitting medium were introduced into the DAC together with the sample. Pressure was monitored by measuring the wavelength shift of the Sm^{2+} line excited by a 100 mW argon laser and detected by a 100 cm Jarrell-Ash optical spectrometer. The precision of pressure measurements was 0.5 kbar. The lattice parameters of four crystals, with dimensions up to $0.12 \times 0.10 \times 0.06$ mm, selected from the same sample and independently mounted in the DAC, were determined at various pressures between 0.001 and 58 kbar by applying the least-squares method to the Bragg angles of about 30 accurately centered reflections in the range 10–300 °θ. The measurements on different crystals allowed us to repeat the compressibility determinations and to investigate the effect due to a different mounting of the sample and a different set of accessible reflections. Unfortunately because of the perfect (100) cleavage of kyanite, all selected crystals had [100] coinciding with the DAC axis, and therefore access to the reciprocal lattice was reduced in this direction.

Diffraction data were collected at room conditions on a Philips PW1100 four-circle diffractometer from a crystal of $0.14 \times 0.10 \times 0.08$ mm, using a graphite monochromater for MoKα radiation (λ = 0.7107 Å); scans with scan width 2.6° and speed in the range 0.04–0.12° s^{-1} were employed. 1940 integrated intensities (up to 350θ) were collected for structural refinement (Table 1). Empirical absorption correction based on the method of North et al. (1968) was applied: transmission factors were in the range 1.0–0.85. A value of 1660 unique reflections with intensities higher than 3σ were employed for the refinement with anisotropic displacement parameter in space group *P* using the SHELX-76 program (Sheldrick 1976) and starting from the atomic coordinates of Burnham (1963). The final agreement index was 2.8% for 146 parameters. The neutral atomic scattering factor values from the *International Tables for X-ray Crystallography* (Ibers and Hamilton 1974) were used.

The intensity data of kyanite were collected at 25.4, 37, and 47 kbar up to 35°, adopting nonbisecting geometry (Denner et al. 1978) and 2.4° ω scans; when possible, the measurements were repeated at different azimutal Ψ angle. Data were corrected for pressure-cell absorption by an experimental attenuation curve (Finger and King 1978). Because systematic errors may be introduced by comparison of refinement results obtained by reflections measured in room conditions belonging to the whole reciprocal lattice with results obtained by reflections mea-

TABLE 2. Atomic fractional coordinates and displacement factors (Å²)

Atom	*x*	*y*	*z*	*U*/*U*eq
Si1	0.2963(1)	0.0649(1)	0.7067(1)	0.0040(1)
	0.297(1)	0.0651(5)	0.7070(7)	0.0052(8)
	0.298(1)	0.0660(5)	0.7073(6)	0.0025(7)
	0.299(2)	0.0660(6)	0.7080(7)	0.0034(8)
	0.298(2)	0.0655(8)	0.7069(9)	0.003(1)
Si2	0.2910(1)	0.3318(1)	0.1892(1)	0.0038(1)
	0.292(2)	0.3321(5)	0.1893(7)	0.0053(8)
	0.292(2)	0.3316(5)	0.1895(6)	0.0031(7)
	0.293(2)	0.3319(5)	0.1892(7)	0.0026(8)
	0.294(2)	0.3325(8)	0.1897(9)	0.003(1)
Al1	0.3254(1)	0.7042(1)	0.4582(1)	0.0047(1)
	0.323(2)	0.7038(5)	0.4582(7)	0.006(1)
	0.326(2)	0.7043(6)	0.4592(7)	0.0037(7)
	0.328(2)	0.7051(7)	0.4600(9)	0.0055(9)
	0.326(3)	0.705(1)	0.458(1)	0.006(1)
Al2	0.2974(1)	0.6988(1)	0.9505(1)	0.0046(1)
	0.298(2)	0.6991(5)	0.9501(7)	0.0061(9)
	0.299(2)	0.6992(5)	0.9506(7)	0.0045(7)
	0.297(2)	0.6989(6)	0.9495(8)	0.0040(8)
	0.295(2)	0.6989(9)	0.950(1)	0.006(1)
Al3	0.0997(1)	0.3861(1)	0.6405(1)	0.0045(1)
	0.101(2)	0.3856(6)	0.6409(7)	0.0052(9)
	0.103(2)	0.3866(6)	0.6403(7)	0.0036(7)
	0.102(2)	0.3867(7)	0.6409(8)	0.0041(9)
	0.102(2)	0.3879(9)	0.641(1)	0.000(1)
Al4	0.1120(1)	0.9174(1)	0.1648(1)	0.0047(1)
	0.111(2)	0.9170(5)	0.1648(8)	0.0053(9)
	0.112(2)	0.9181(5)	0.1652(7)	0.0037(8)
	0.113(2)	0.9184(7)	0.1653(8)	0.0053(9)
	0.110(2)	0.9144(8)	0.163(1)	0.001(1)
O1	0.1094(2)	0.1469(2)	0.1288(2)	0.0054(2)
	0.104(4)	0.146(1)	0.128(2)	0.01(2)
	0.108(4)	0.148(1)	0.132(2)	0.006(2)
	0.109(5)	0.148(2)	0.130(2)	0.011(3)
	0.119(5)	0.150(2)	0.134(2)	0.002(3)
O2	0.1231(2)	0.6855(1)	0.1815(2)	0.0049(2)
	0.130(5)	0.686(1)	0.184(2)	0.003(2)
	0.129(4)	0.687(1)	0.184(2)	0.003(2)
	0.128(5)	0.685(1)	0.181(2)	0.003(2)
	0.116(6)	0.680(2)	0.181(2)	0.001(3)
O3	0.2750(2)	0.4546(1)	0.9546(2)	0.0058(3)
	0.272(3)	0.454(1)	0.954(1)	0.004(2)
	0.272(3)	0.455(1)	0.956(1)	0.004(2)
	0.276(4)	0.454(1)	0.951(2)	0.005(2)
	0.280(5)	0.455(2)	0.953(1)	0.002(3)
O4	0.2832(2)	0.9356(1)	0.9357(2)	0.0056(3)
	0.282(4)	0.935(1)	0.934(2)	0.006(2)
	0.283(4)	0.936(1)	0.936(2)	0.004(2)
	0.283(4)	0.933(2)	0.935(2)	0.008(2)
	0.278(5)	0.934(2)	0.937(2)	0.000(3)
O5	0.1083(2)	0.1521(2)	0.6666(2)	0.0052(2)
	0.106(5)	0.150(1)	0.664(2)	0.004(2)
	0.110(5)	0.151(1)	0.665(2)	0.008(2)
	0.113(5)	0.152(1)	0.666(2)	0.002(2)
	0.119(6)	0.155(2)	0.667(2)	0.002(3)
O6	0.1221(2)	0.6306(2)	0.6390(2)	0.0051(2)
	0.119(4)	0.629(1)	0.637(2)	0.005(2)
	0.118(4)	0.631(1)	0.638(2)	0.004(2)
	0.115(5)	0.629(2)	0.638(2)	0.012(3)
	0.121(5)	0.633(2)	0.640(2)	0.001(3)
O7	0.2823(2)	0.4452(2)	0.4288(2)	0.0058(3)
	0.284(4)	0.445(1)	0.429(2)	0.009(2)
	0.285(4)	0.446(1)	0.429(2)	0.004(2)
	0.284(4)	0.444(2)	0.429(2)	0.012(3)
	0.287(5)	0.447(2)	0.429(2)	0.000(3)
O8	0.2914(2)	0.9469(1)	0.4659(2)	0.0058(3)
	0.292(3)	0.948(1)	0.463(1)	0.005(2)
	0.292(3)	0.947(1)	0.465(1)	0.006(2)
	0.292(4)	0.946(1)	0.465(1)	0.004(2)
	0.291(5)	0.946(2)	0.462(2)	0.003(3)
O9	0.5007(2)	0.2751(2)	0.2447(2)	0.0055(3)
	0.499(4)	0.277(1)	0.245(2)	0.008(2)
	0.499(4)	0.275(1)	0.245(2)	0.004(2)
	0.504(5)	0.275(2)	0.245(2)	0.010(2)
	0.511(6)	0.273(2)	0.247(2)	0.005(3)
O10	0.5012(2)	0.2310(2)	0.7561(2)	0.0053(3)
	0.494(6)	0.231(2)	0.753(2)	0.005(2)
	0.498(5)	0.232(1)	0.754(2)	0.004(2)
	0.499(6)	0.232(2)	0.753(2)	0.001(2)
	0.511(7)	0.237(2)	0.758(2)	0.005(3)

Note: For each atom, values from top to bottom correspond to the refinement at 0.001, 0.1, 25.4, 37, and 47 kbar respectively. Estimated standard deviations are in parentheses and refer the last digit. For H*P* refinements the isotropic thermal parameters (*U*) is reported, whereas for the room condition refinement U_{eq} is shown.

sured from a limited part of the reciprocal space within the DAC, the same set of intensity data was collected at 0.1 kbar from the same crystal with the use of the same procedure.

Intensity data were analyzed with a digital procedure (Comodi et al. 1994) and visually inspected to eliminate errors due to the overlap of diffraction effects from various components of the DAC or to shadowing by the gasket. Reflections measured at different Ψ angles were then merged to form an independent data set.

The structure was refined with individual isotropic atomic displacement parameters. Final *R* values were 8.2, 5.9, 6.8, and 8.0% for 364, 373, 359, and 343 independent observed reflections and 65 parameters, respectively, for refinements at 0.1, 25.4, 37, and 47 kbar. Details of refinements are listed in Table 1 and resulting fractional atomic positions and thermal parameters are given in Table 2. Observed and calculated structure factors are listed in Table 3[1].

RESULTS AND DISCUSSION

Compressibility

Unit-cell parameters of kyanite are given as a function of pressure in Table 4 and in Figure 1. As is clear from the standard deviation of the measurements, both lattice parameter *a* and β and γ angles were determined with a precision less than that of the other cell parameters because of the mounting of the crystal in the DAC. Kyanite deformed linearly in the pressure range examined, following an almost isotropic compression pattern. Linear regressions yielded mean axial compressibilities for *a*, *b*, and *c* axes of $2.00(8) \times 10^{-4}$, $1.90(4) \times 10^{-4}$ and $2.00(4) \times 10^{-4}$ kbar^{-1} respectively. The linear volume compressibility was $5.8(1) \times 10^{-4}$ kbar^{-1}, with $K = 1720(30)$ kbar (Fig. 2).

The principal axes of the strain ellipsoid were calculated with the STRAIN program (Ohashi 1982), using lattice parameter values from regression equations. The principal strain axes, reported in Table 5 with their orientation with respect to the unit-cell axes, show a com-

[1] A copy of Table 3 may be ordered as Document AM-97-637 from the Business Office, Mineralogical Society of America, 1015 Eighteenth Street, NW, Suite 601, Washington DC 20036 USA. Please remit $5.00 in advance for the microfiche.

TABLE 4. Lattice parameters of kyanite at different pressures

Sample	*P* (kbar)	*a* (Å)	*b* (Å)	*c* (Å)	α (°)	β (°)	γ (°)	*V* (Å³)
I	0.001	7.124(2)	7.856(2)	5.577(2)	89.99(2)	101.15(2)	105.95(2)	293.9(3)
I	0.1	7.117(5)	7.860(3)	5.575(2)	90.02(3)	101.02(5)	106.06(5)	293.7(4)
I	7.9	7.106(5)	7.848(3)	5.566(2)	90.07(3)	100.96(5)	106.03(5)	292.4(4)
I	15.2	7.100(5)	7.837(3)	5.556(2)	90.11(3)	100.91(5)	106.06(5)	291.2(4)
I	25.4	7.079(5)	7.824(3)	5.547(2)	90.13(3)	101.00(5)	105.98(5)	289.4(4)
I	23.8	7.083(5)	7.825(3)	5.549(2)	90.11(3)	101.02(5)	106.00(5)	289.7(4)
I	33.0	7.068(5)	7.811(3)	5.538(2)	90.13(3)	101.00(5)	105.98(5)	288.0(4)
I	37.0	7.065(5)	7.805(3)	5.537(2)	90.12(3)	101.08(5)	105.86(5)	287.7(4)
II	0.1	7.107(5)	7.858(3)	5.576(2)	90.06(3)	100.74(5)	105.95(5)	293.7(4)
II	4.5	7.118(5)	7.848(3)	5.578(2)	90.01(3)	101.10(5)	105.99(5)	293.5(4)
II	11.5	7.110(5)	7.837(3)	5.571(2)	90.02(3)	101.08(5)	105.97(5)	292.4(4)
III	14.4	7.104(5)	7.830(3)	5.565(2)	90.02(3)	101.08(5)	105.98(5)	291.6(4)
III	15.8	7.099(5)	7.821(3)	5.560(2)	90.06(3)	101.13(5)	105.90(5)	290.8(4)
IV	30.5	7.088(5)	7.804(3)	5.539(2)	90.11(3)	101.30(5)	105.99(5)	288.3(4)
IV	34.5	7.077(5)	7.803(3)	5.536(2)	90.09(3)	101.29(5)	106.03(5)	287.6(4)
IV	39.5	7.063(5)	7.796(3)	5.528(2)	90.13(3)	101.09(5)	105.92(5)	286.7(4)
IV	41.5	7.050(5)	7.796(3)	5.532(2)	90.14(3)	101.03(5)	106.00(5)	286.4(4)
IV	42.5	7.053(5)	7.788(3)	5.528(2)	90.12(3)	101.01(5)	106.00(5)	286.1(4)
IV	48.0	7.056(5)	7.785(3)	5.525(2)	90.13(3)	101.14(5)	105.90(5)	285.9(4)
IV	46.0	7.070(5)	7.783(3)	5.524(2)	90.14(3)	101.19(5)	105.81(5)	286.5(4)
IV	50.0	7.052(5)	7.783(3)	5.524(2)	90.18(3)	101.18(5)	105.90(5)	285.6(4)
IV	52.0	7.052(5)	7.782(3)	5.521(2)	90.17(3)	101.20(5)	105.90(5)	285.4(4)
IV	58.0	7.031(5)	7.776(3)	5.517(2)	90.16(3)	101.15(5)	105.90(5)	284.1(4)

pression pattern more anisotropic than that of the cell edges, ratios β_1:β_2:β_3 being 1.4:1.2:1.

The compressibility distribution may be related to the hardness pattern after the inverse relationship proposed by Yang et al. (1987). Buttgenbach (1923) showed that, in kyanite, hardnesses determined parallel to [001] on both (100) and (010) planes were less than those measured normal to [001] by about one unit on the Mohs scale. The compressibility pattern found here partly explains the hardness pattern: the greatest compressibility and smallest hardness are found approximately along [001].

Isothermal bulk modulus K_0 and its pressure derivative K' were found by fitting the pressure-volume data to a third-order Birch-Murnaghan equation of state (Birch 1978). The equation has the form:

$$P = 3/2K_0\,[(V_0/V)^{7/3} - (V_0/V)^{5/3}]$$

$$\{1 + 3/4(K' - 4)[(V_0/V)^{2/3} - 1]\}$$

and was solved using a Levenberg-Marquardt algorithm (Press et al. 1986). K_0 was 1560(100) kbar and K' was 5.6(5.5), with a reference volume V_0 of 293.92(9) Å³. When K' was set at 4, K_0 became 1600(30) kbar. The bulk modulus, calculated as the reciprocal of average volume compressibility, obtained by the linear least-squares fit of volume-pressure data, was 1720(30) kbar.

The K_0 value compares well with the bulk moduli of other compact phases such as pyrope, with K_0 = 1430–1750 kbar (Hazen and Finger 1978; Levien et al. 1979). In effect, if structural compactness is expressed in terms of the volume occupied by one O atom in the unit cell, the value for kyanite is 14.7 Å³, that for pyrope is 15.7 Å³, and the value for corundum is 14.2 Å³. In the silica phases, the O volume decreases from 18.8 to 17.1 and to 11.6 Å³ for α-quartz, coesite, and stishovite, respectively.

Previous determinations of the compressibility of aluminosilicates were made by Brace et al. (1969) on hot-pressed synthetic aggregates. For kyanite they found a compressibility value of about 0.65 Mbar^{-1} (K_0 = 1540 kbar), higher than our value of 0.58 Mbar^{-1}. As reported by the above authors, the compressibility data obtained from pressed materials may be overestimated because of porosity. Our K_0 value (1560 kbar) shows excellent agreement with that determined by Marsh (1980) with wave method: K_s = 1560 (100) kbar. K_0 inferred from thermodynamic data in the study of Irifune et al. (1995), 2020(100)kbar, is significantly higher than that observed in either Marsh's (1980) study or this study.

The bulk modulus of kyanite is about 15% larger than that of andalusite, the low-temperature, low-pressure polymorph of aluminosilicate. Ralph et al. (1984) measured a value of 1350 kbar for this phase.

Pressure induced changes on kyanite structure

The results of refinement of kyanite in air (Table 2) are very similar to those of Winter and Ghose (1979). The structure of kyanite is based on a distorted cubic close-packing of O atoms, with 10% of the tetrahedral sites filled with Si and 40% of the octahedral sites with Al. The structure can be described as infinite chains composed of a sequence of Al1 and Al2 octahedra parallel to the *c* axis, with Al3 and Al4 octahedra on alternate sides of the chains. The octahedral chains are linked by isolated Si tetrahedra. This octahedral configuration gives rise to ten independent shared octahedral edges: Al1 and Al3 share five edges with neighboring octahedra, whereas Al2 and Al4 have four shared edges with other octahedra. On the whole, there are a great number of shared edges uniformly distributed in the unit cell, and this may explain the almost isotropic compressibility of the phase.

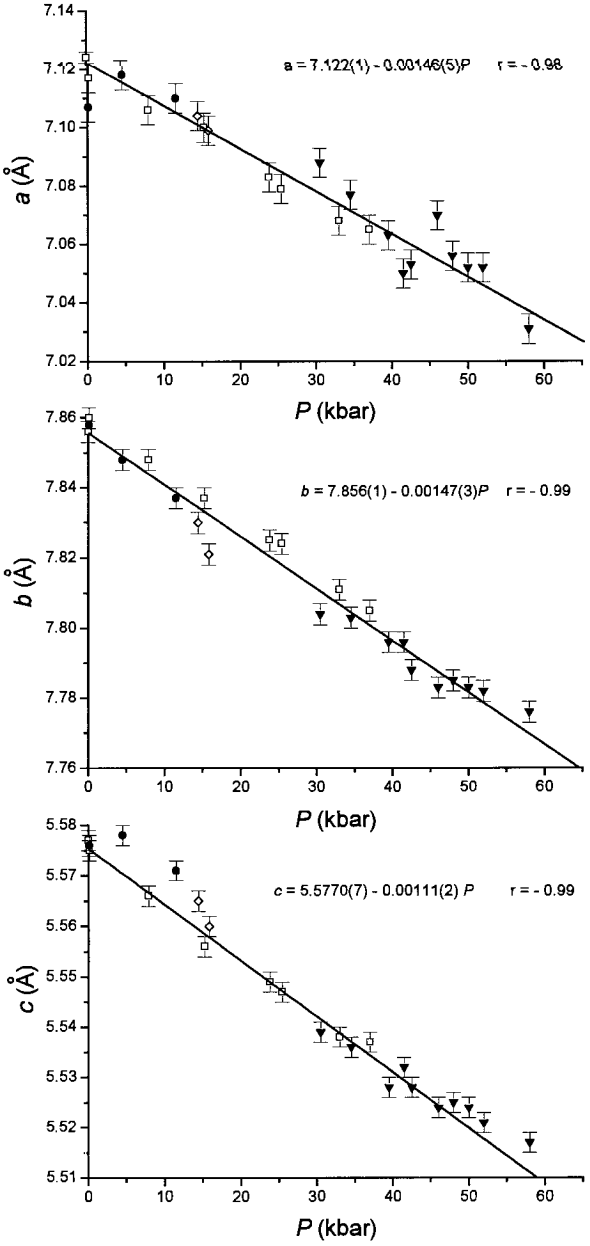

FIGURE 1. Unit-cell parameters *a*, *b*, and *c* of kyanite vs. pressure. Open squares: sample I; full circles: sample II; diamonds: sample III; full triangles: sample IV. Error for pressure: about 0.5 kbar. Top right: regression line equation.

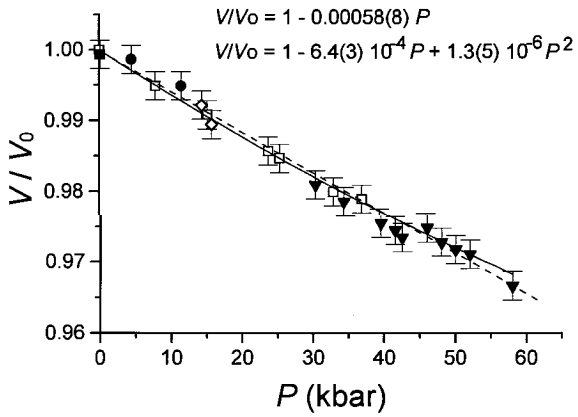

FIGURE 2. V/V_o as a function of *P*. Symbols as in Fig. 1. Dashed line: linear fit of volume-pressure data; continuous line: fit with a quadratic curve.

To examine structural evolution with pressure more in detail, we may compare the structural refinements obtained with data collected at 0.1, 25.4, 37, and 47 kbar, as well as in room conditions. The results are as follows. (1) The Si1 and Si2 silicon tetrahedra do not change with increased pressure, either as regards the average bond distances or the polyhedral volumes (Tables 6 and 7); this result is normal in silicates in this pressure range. (2) In room conditions, the four crystallographically independent Al octahedra show a limited variational range both in average bond lengths (from 1.897 Å of Al4 to 1.918 Å of Al3) and in volumes [(from 8.93(1) Å^3 of Al4 to 9.17(1) Å^3 of Al3)]. However, with increased pressure the behavior of the four polyhedra changes. The average bulk moduli for the various polyhedra calculated from linear regressions are the same for Al1 and Al2, equal to 1280(150) kbar, and equal to 2380(200) kbar for Al3. The Al4 octahedron turns out to be incompressible. In effect, the ⟨Al4-O⟩ mean distance is very short, smaller than the sum of the ionic radii of Al and O (1.915 Å; Shannon 1976). Also in other structures, for example clinozoisite (Comodi and Zanazzi 1997), Al octahedra with short Al-O distances are incompressible in this pressure range, whereas the Al3 octahedron, in spite of its larger average bond distance, has a bulk modulus about twice that of Al1 and Al2.

Octahedral bond lengths decrease with pressure at a rate which is sometimes independent of bond strength. That is, some shorter distances, with higher bond strengths, decrease with *P* more than the longer ones. This is the case, for example, of the short Al1-O9 and Al1-O10 (Table 6) which decrease more than the longer Al1-O7. Nevertheless, on the whole, Al octahedra tend to become more regular with pressure. Table 7 lists the linear and angular distortions as calculated with Robinson's relationship (Robinson et al. 1971) for all polyhedra. In the Al2, Al3, and Al4 octahedra, a trend toward regularization with pressure is evident, especially the angular distortion. Since the octahedra form a complex arrangement sharing edges, the structural evolution with *P* must

TABLE 5. Principal strain components of compressibility

Principal strain components (per kbar × 10^{-4})	Orientation of principal axes (°) with respect to		
	a	*b*	*c*
2.23	101	54	37
2.04	14	106	88
1.65	82	40	127

TABLE 6. Bond distances (Å) of kyanite at different pressures

P (kbar)	0.001	0.1	25.4	37	47
Si1-O5	1.644(2)	1.65(3)	1.62(3)	1.61(4)	1.58(4)
Si1-O10	1.645(1)	1.61(3)	1.61(2)	1.62(3)	1.69(3)
Si1-O4	1.632(1)	1.63(1)	1.63(1)	1.63(1)	1.64(2)
Si1-O8	1.621(1)	1.63(1)	1.62(1)	1.62(1)	1.62(2)
⟨Si1-O⟩	1.635	1.63	1.62	1.62	1.63
Si2-O1	1.642(1)	1.67(2)	1.63(2)	1.64(2)	1.59(2)
Si2-O7	1.627(2)	1.62(1)	1.61(1)	1.61(2)	1.61(2)
Si2-O9	1.647(2)	1.62(3)	1.63(3)	1.64(4)	1.69(4)
Si2-O3	1.630(1)	1.63(1)	1.63(1)	1.63(1)	1.62(1)
⟨Si2-O⟩	1.636	1.63	1.63	1.63	1.63
Al1-O2	1.872(1)	1.83(2)	1.84(2)	1.86(3)	1.88(3)
Al1-O6	1.885(1)	1.88(3)	1.89(2)	1.91(3)	1.88(3)
Al1-O7	1.975(2)	1.98(1)	1.97(1)	1.97(1)	1.96(2)
Al1-O8	1.988(1)	1.99(1)	1.98(1)	1.96(2)	1.96(2)
Al1-O9	1.845(1)	1.86(2)	1.84(2)	1.80(2)	1.78(2)
Al1-O10	1.854(1)	1.88(3)	1.85(3)	1.83(3)	1.79(4)
⟨Al1-O⟩	1.903	1.90	1.89	1.89	1.88
Al2-O3	1.881(1)	1.89(1)	1.87(1)	1.87(1)	1.87(2)
Al2-O4	1.892(1)	1.89(1)	1.89(1)	1.86(2)	1.87(2)
Al2-O6	1.913(1)	1.94(2)	1.92(1)	1.92(2)	1.88(2)
Al2-O2	1.939(2)	1.91(3)	1.91(3)	1.90(3)	1.94(4)
Al2-O10	1.923(1)	1.96(2)	1.93(2)	1.93(2)	1.87(3)
Al2-O9	1.934(2)	1.93(2)	1.92(3)	1.90(3)	1.88(4)
⟨Al2-O⟩	1.914	1.92	1.91	1.90	1.89
Al3-O3	1.924(1)	1.92(1)	1.90(1)	1.89(1)	1.90(2)
Al3-O5	1.861(2)	1.86(2)	1.86(2)	1.86(2)	1.86(2)
Al3-O6	1.883(2)	1.88(1)	1.88(1)	1.87(2)	1.87(2)
Al3-O7	1.888(1)	1.89(2)	1.87(2)	1.87(3)	1.89(3)
Al3-O2	1.985(1)	2.01(3)	2.02(3)	2.01(3)	1.94(4)
Al3-O6	1.969(1)	1.96(2)	1.95(2)	1.93(3)	1.96(3)
⟨Al3-O⟩	1.918	1.92	1.91	1.90	1.90
Al4-O2	1.847(1)	1.86(2)	1.85(2)	1.85(2)	1.84(2)
Al4-O8	1.875(1)	1.88(1)	1.86(1)	1.86(2)	1.85(2)
Al4-O1	1.819(2)	1.82(1)	1.81(1)	1.81(2)	1.83(2)
Al4-O4	1.910(2)	1.91(2)	1.90(2)	1.90(3)	1.86(3)
Al4-O5	1.935(1)	1.91(3)	1.94(3)	1.95(3)	1.98(4)
Al4-O1	1.997(1)	1.98(2)	1.99(2)	1.99(2)	2.03(2)
⟨Al4-O⟩	1.897	1.89	1.89	1.89	1.90

be analyzed by determining the Al-Al separation across the shared edges. Looking at the changes in Al-Al separation (Table 8) an unexpected result stands out: the largest reduction involves Al2-Al3 and Al2-Al4, whereas the average distances between Al1-Al2, the two most compressible octahedra, remain almost unchanged. In fact, the Al1 and Al2 octahedra are linked along the *c* axis by tetrahedral edges O8-O4 and O7-O3 (see Fig. 11 in Winter and Ghose 1979), which do not change with pressure: O4-O8 is 2.64(1) Å at 0.1 kbar and 2.65(2) at 47 kbar, and O3-O7 is 2.63(1) Å at 0.1 kbar and 2.62(2) Å at 47 kbar. So the reduction of the distance between Al1 and Al2 does not occur along the *c* axis, but along the Al4-Al1-Al3 and Al4-Al2-Al3 directions.

High-pressure high-temperature behavior

Thermal expansion data obtained from single-crystal X-ray diffraction by Winter and Ghose (1979) and those previously determined by powder diffraction by Skinner et al. (1961) allow us to compare the structural behavior of kyanite with different intensive variables and to verify whether the antisymmetric behavior observed in many crystal structures (e.g., Hazen and Finger 1982) is also followed by this phase.

The thermal strain ellipsoid for kyanite determined between 25 and 800 °C by Winter and Ghose (1979), shows a slightly more anisotropic strain with respect to the compressibility strain, with $\alpha_1:\alpha_2:\alpha_3 = 1.8:1.4:1$. The largest thermal expansion coefficient forms an angle of about 15° with the *c* axis. So with *T* and *P* the largest variation occurs along a direction forming a small angle with the *c* axis.

By comparing our data with those of Winter and Ghose (1979), the inverse relationship is observed in all geometrical parameters. The α angle increases with *P* whereas it decreases with *T*. The angles β and γ remain almost unchanged with *P* as well as with the *T* increase. Whereas the octahedra become more regular with pressure, their distortion in terms of both longitudinal and shear strain increases with temperature.

Assuming that the variations induced by *T* and *P* are cumulative and that $(\partial\alpha/\partial P)_T$ and $(\partial\beta/\partial T)_P$ derivatives are zero, we may determine the conditions that do not change the structure with respect to room conditions, at least from the volumetric point of view. The β_V/α_V ratio, obtained from the cell volume average compressibility and

TABLE 7. Polyhedral volumes (Å³), distortion parameters, and polyhedral bulk moduli (kbar) of kyanite

P (kbar)	0.001	0.1	25.4	37	47	*K*
VSi1	2.242(4)	2.22(8)	2.18(8)	2.17(8)	2.23(9)	—
⟨λ⟩	1.00	1.00	1.00	1.00	1.00	
δ²	4.6	6.4	6.2	8.9	7.2	
VSi2	2.243(4)	2.24(8)	2.20(8)	2.22(8)	2.21(8)	—
⟨λ⟩	1.00	1.00	1.00	1.00	1.00	
δ²	7.1	8.9	8.5	5.3	7.8	
VAl1	8.99(1)	9.0(2)	8.8(2)	8.8(2)	8.6(2)	1280(150)
⟨λ⟩	1.02	1.01	1.01	1.02	1.02	
δ²	47.7	40.0	44.8	50.6	53.6	
VAl2	9.15(1)	9.2(2)	9.0(2)	8.9(2)	8.8(3)	1280(150)
⟨λ⟩	1.01	1.01	1.01	1.01	1.01	
δ²	50.8	58.4	49.9	47.7	46.4	
VAl3	9.17(1)	9.2(2)	9.1(2)	9.0(2)	9.0(3)	2380(200)
⟨λ⟩	1.02	1.02	1.02	1.02	1.02	
δ²	57.0	58.4	57.8	52.4	48.6	
VAl4	8.93(1)	8.9(2)	8.9(2)	8.9(2)	8.9(3)	—
⟨λ⟩	1.01	1.01	1.00	1.01	1.01	—
δ²	42.0	42.0	42.6	45.9	37.8	

Note:

$$\langle\lambda\rangle = \sum_{i=1}^{n} [(l_i/l_0)^2/n]$$

$$\delta^2 = \sum_{i=1}^{n} [(\theta_i - \theta_0)^2/(n-1)]$$

TABLE 8. Al-Al separation (Å)

P (kbar)	0.001	0.1	25.4	37	47
Al1-Al4	2.869(1)	2.87(1)	2.87(1)	2.86(1)	2.83(2)
Al1-Al3	2.879(1)	2.867(8)	2.852(9)	2.86(1)	2.85(1)
Al2-Al3	2.858(1)	2.864(6)	2.841(6)	2.829(7)	2.814(9)
Al2-Al4	2.825(1)	2.82(1)	2.82(1)	2.80(1)	2.77(1)
Al1-Al2	2.791(1)	2.781(7)	2.768(7)	2.760(9)	2.77(1)
Al1-Al2	2.799(1)	2.805(6)	2.791(6)	2.792(7)	2.770(9)
Al3-Al3′	2.866(1)	2.89(1)	2.87(1)	2.86(1)	2.84(2)
Al1-Al3	2.855(1)	2.84(2)	2.86(2)	2.86(2)	2.85(2)
Al3-Al4	2.792(1)	2.781(8)	2.792(8)	2.79(1)	2.77(1)
Al4-Al4′	2.759(1)	2.76(1)	2.74(1)	2.74(1)	2.74(2)

the average thermal expansion as determined by Winter and Ghose (1979), is 23 °C/kbar. This result is similar to that measured for high-pressure minerals such as magnesiochloritoid (Comodi et al. 1992), for which the geometric invariance condition is obtained at gradients of about 23 °C/kbar, or for lawsonite (Comodi and Zanazzi 1996) with a gradient of 29 °C/kbar.

The observed antisymmetric behavior of kyanite with T and P shows that, at first approximation, the effects of pressure and temperature are additive, and the following equation of state may be defined: $V/V_o = 1 + 3.00(7) \times 10^{-5}\ T - 5.8(1) \times 10^{-4}\ P$, where T is in °C and P in kbar. This equation may be applied at crustal P-T conditions.

The stability of kyanite

Kyanite decomposes with increasing pressure to its constituents stishovite and corundum between 140 kbar at 1000 °C and 175 kbar at 2000 °C (Schmidt et al. 1997) through a reaction with a gently positive dP/dT slope with kyanite lies on the high-temperature, low-pressure side of the reaction. Lower pressures (120–130 kbar, depending on temperature) for breakdown of kyanite were observed by Irifune et al. (1995). On the contrary at low pressure Harlov and Newton (1993) reversed the metastable equilibrium kyanite = corundum + quartz which again has a positive dP/dT slope, but with kyanite is on the low-temperature, high-pressure side of the reaction. Such metastable reaction has been claimed to be of significance in natural occurrences for high-grade metamorphic rocks (Harlov and Newton 1993, and references therein).

New volume properties of kyanite may help to unravel reaction mechanisms which determine the stability field of kyanite and its breakdown reactions at both low and high pressure. Figure 3a shows the evolution with pressure of molar volumes of kyanite compared with those of corundum + quartz, corundum + coesite, and corundum + stishovite (see Schmidt et al. 1997, for the data used). As long as quartz or coesite are present in association with corundum, kyanite should be favored on the high-pressure side of decomposition reactions by a significantly lower volume.

Coesite-stishovite transformation causes a decrease of the volume for the assemblage corundum + SiO_2 in the order of 10%, and purely from a geometrical point of view, the breakdown of kyanite should occur. Despite such volumetric handicap, kyanite persists more than 40 kbar in excess of coesite-stishovite transition. This behavior can be explained by entropy properties of SiO_2 polymorphs. Figure 3b demonstrates that coesite-stishovite transition causes a large decrease of the entropy for corundum + SiO_2, which becomes much lower than that of kyanite. Thus, the relatively high entropy of kyanite counterbalances its relatively large volume and kyanite is stable as long as the free energy function for kyanite is lower than the one for corundum + stishovite.

Because of the large ΔV and ΔS of the reaction coesite to stishovite and because of their opposite sign, the breakdown reaction kyanite = corundum + SiO_2 conserves the sign of dP/dT slope both in quartz, and in coesite, and in stishovite stability fields, but products and reactants should interchange at coesite-stishovite transformation.

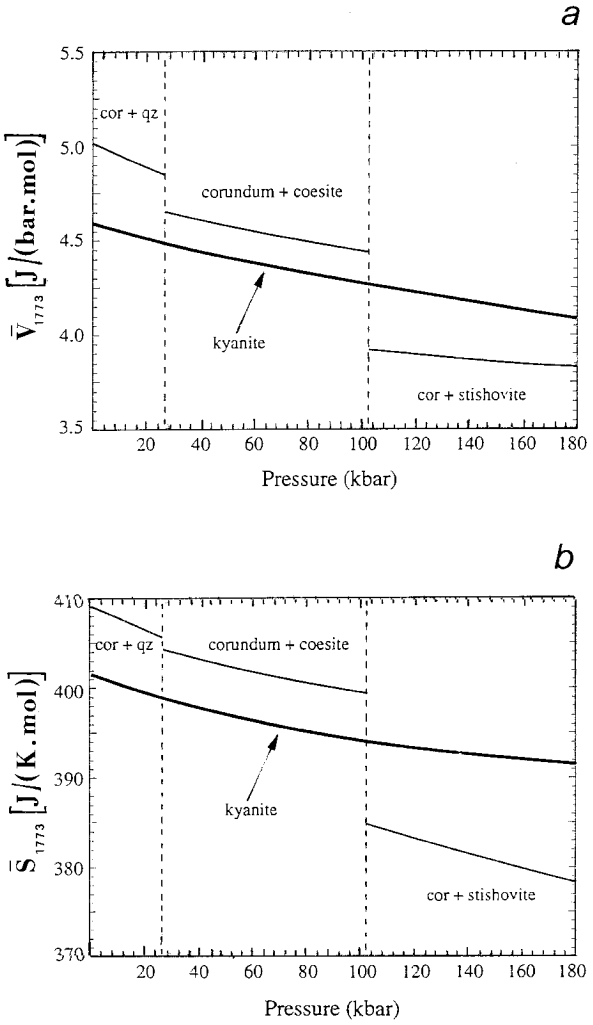

FIGURE 3. **(a)** Molar volumes (J/kbar) vs pressure (bar) of corundum + quartz, corundum + coesite, kyanite, and corundum + stishovite calculated at 1500 °C. (**b**) Molar entropy, S (J/K) vs. P (kbar) of corundum + silica polymorphs and kyanite. Data for reaction kyanite ↔ corundum + stishovite from Schmidt et al. (1997). Steps correspond to pressures at which quartz ↔ coesite and coesite ↔ stishovite transitions take place. See Schmidt et al. (1997) for references.

ACKNOWLEDGMENTS

We would like to thank R.T. Downs for kindly providing the program for the Birch Murnaghan fit. This work was supported by CNR and MURST (ex 40% and 60% funds) grants to PFZ.

REFERENCES CITED

Ahmed-Zäid, I. and Madon, M. (1991) A high-pressure form of Al_2SiO_5 as a possible host of aluminum in the lower mantle. Nature, 353, 426–428.

Birch, F. (1978) Finite strain isotherm and velocities for single-crystal and

polycrystalline NaCl at high pressures and 300 K. Journal of Geophysical Research, 83, 1257–1267.

Brace, W.F., Scholz, C.H., and La Mori, P.N. (1969) Isothermal Compressibility of Kyanite, Andalusite and Sillimanite from Synthetic Aggregates. Journal of Geophysical Research, 74, 2089–2098.

Burnham, C.W. (1963) Refinement of the crystal structure of kyanite. Zeitschrift für Kristallographie, Bd 118, 337–360.

Buttgenbach, H. (1923) Description des minéraux du Congo belge (Sixiéme Memoire) Memoires de l'Academie du Royaume de Belgique. Classe de Sciences, 2, 7, 6. [Mineralogical Abstracts 2–265].

Chatterjee, N.D. (1972) The upper stability limit of the assemblage paragonite + quartz and its natural occurrences. Contributions to Mineralogy and Petrology, 34, 288–303.

Comodi, P., Mellini, M., and Zanazzi, P.F. (1992) Magnesiochloritoid, Compressibility and high pressure structure refinement. Physics and Chemistry of Minerals, 18, 483–490.

Comodi, P. and Zanazzi, P.F. (1993) Improved calibration curve for the Sm^{2+}, BaFCl pressure sensor. Journal of Applied Crystallography, 26, 843–845.

Comodi, P., Melacci, P.T., Polidori, G., and Zanazzi, P.F. (1994) Trattamento del profilo di diffrazione da campioni in cella ad alta pressione. Proceedings of XXIV National Congress of Associazione Italiana di Cristallografia. Pavia, September 27-29, 119–120.

Comodi, P. and Zanazzi, P.F. (1996) Effects of temperature and pressure on the structure of lawsonite. American Mineralogist, 81, 833–841.

———(1997) The pressure behavior of clinozoisite and zoisite: an X-ray diffraction study. American Mineralogist, 82, 61–68.

Denner, W., Schulz, H., and d'Amour, H. (1978) A new measuring procedure for data collection with a high-pressure cell on X-ray four-circle diffractometer. Journal of Applied Crystallography, 11, 260–264.

Finger, L.W. and King, H. (1978) A revised method of operation of the single-crystal diamond cell and refinement of the structure of NaCl at 32 kbar. American Mineralogist, 63, 337–342.

Harlov, D.H. and Newton, R.C. (1993) Reversal of the metastable kyanite + corundum + quartz and andalusite + corundum + quartz equilibria and the enthalpy of formation of kyanite and andalusite. American Mineralogist, 78, 594–600.

Hazen, R.M. and Finger, L.W. (1978) Crystal structures and compressibilities of pyrope and grossular to 60 kbar. American Mineralogist, 63, 297–303.

———(1982) Comparative Crystal Chemistry, 228 p. Wiley, New York.

Ibers, J.A. and Hamilton, W.C., Eds. (1974) International tables for X-ray crystallography, vol. IV, 366 p. Kynoch, Birmingham, U.K.

Irifune, T., Kuroda, K., Minagawa, T, and Unemoto, M. (1995) Experimental study of the decomposition of kyanite at high pressure and high temperature. In T. Yukutake, Ed., The Earth's central part: its structure and dynamics, p. 35–44. Terra Scientific Publishing Company (Terrapub), Tokyo.

Levien, L., Prewitt, C.T., and Weidner, D.J. (1979) Compression of pyrope. American Mineralogist, 64, 805–808.

Liu, L.G. (1974) Disproportion of kyanite to corundum plus stishovite at high pressure and temperature. Earth and Planetary Science Letters, 24, 224–228.

Marsh, S.P. (1980) LASL Shock Hugoniot data, 658 p. University of California Press, Berkeley.

North, A.C.T., Phillips, D.C., and Mathews, F.S. (1968) A semiempirical method of absorption correction. Acta Crystallographica, A24, 351–359.

Ohashi, Y. (1982) A program to calculate the strain tensor from two sets of unit-cell parameters. In: Comparative Crystal Chemistry. Eds. R.M.Hazen and L.W. Finger. Wiley, New York., 92–102.

Poli, S. and Schmidt, M.W. (1995) H_2O transport and release in subduction zones: Experimental constraints on basaltic and andesitic systems. Journal of Geophysical Research, 100, 22299–22314.

Press, W.H., Flannery, B.P., Teukolsky, S.A., and Vetterling, W.T. (1986) Numerical recipes, 521–528. Cambridge University Press, Cambridge, UK.

Ralph, R.L., Finger, L.W., Hazen, R.M., and Ghose, S. (1984) Compressibility and crystal structure of andalusite at high pressure. American Mineralogist, 69, 513–519.

Ringwood, A.E. (1991) Phase transformations and their bearing on the constitution and dynamics of the mantle. Geochimica and Cosmochimica Acta, 55, 2083–2110.

Ringwood, A.E. and Reid, A.F. (1969) High-pressure phase transition of spinel. Earth and Planetary Science Letters, 5, 245.

Robinson, K., Gibbs, G.V., and Ribbe, P.H. (1971) Quadratic elongation: a quantitative measure of distortion in coordination polyhedra. Science, 172, 567–570.

Schmidt, M.W., Poli, S., Comodi, P., and Zanazzi, P.F. (1997) The high pressure behavior of kyanite: decomposition of kyanite into stishovite and corundum. American Mineralogist, 82, 460–466.

Schreyer, W. (1988) Experimental studies on metamorphism of crustal rocks under mantle pressures. Mineralogical Magazine 52, 1–26.

Shannon, R.D. (1976) Revised effective ionic radii and systematic studies of interatomic distances in halides and chalcogenides. Acta Crystallographica, A32, 751–767.

Sheldrick, G.M. (1976) SHELX-76. Program for crystal structure determination. University of Cambridge, Cambridge, UK.

Skinner, B.J., Clark, S.P., and Appleman, D.E. (1961) Molar volumes and thermal expansion of andalusite, kyanite, and sillimanite. American Journal of Science, 259, 651–668.

Yang, W., Parr, R.G., and Uytterhoeven, L. (1987) New relation between hardness and compressibility of minerals. Physics and Chemistry of Minerals 15, 191–195.

Winter, J.K. and Ghose, S. (1979) Thermal expansion and high-temperature crystal chemistry of the Al_2SiO_5 polymorphs. American Mineralogist, 64, 573-586.

Manuscript received June 24, 1996
Manuscript accepted January 14, 1997